# Walsh-Hadamard Neural Operators for Solving PDEs with Discontinuous Coefficients

Giorgio M. Cavallazzi<sup>a,\*</sup>, Miguel Pérez Cuadrado<sup>a</sup>, Alfredo Pinelli<sup>a</sup>

<sup>a</sup>Department of Engineering, City St George's, University of London, Northampton Square, London, EC1V 0HB, UK

## Abstract

Neural operators have emerged as powerful tools for learning solution operators of partial differential equations (PDEs). However, standard spectral methods based on Fourier transforms struggle with problems involving discontinuous coefficients due to the Gibbs phenomenon and poor representation of sharp interfaces. We introduce the Walsh-Hadamard Neural Operator (WHNO), which leverages Walsh-Hadamard transforms—a spectral basis of rectangular wave functions naturally suited for piecewise constant fields—combined with learnable spectral weights that transform lowsequency Walsh coefficients to capture global dependencies efficiently. We validate WHNO on three problems: steady-state Darcy flow (preliminary validation), heat conduction with discontinuous thermal conductivity, and the 2D Burgers equation with discontinuous initial conditions. In controlled comparisons with Fourier Neural Operators (FNO) under identical conditions, WHNO demonstrates superior accuracy with better preservation of sharp solution features at material interfaces. Critically, we discover that weighted ensemble combinations of WHNO and FNO achieve substantial improvements over either model alone: for both heat conduction and Burgers equation, optimal ensembles reduce mean squared error by 35-40\% and maximum error by up to 25% compared to individual models. This demonstrates that Walsh-Hadamard and Fourier representations capture complementary aspects of discontinuous PDE solutions, with WHNO excelling at sharp interfaces while FNO captures smooth features effectively.

Email address: Giorgio.Cavallazzi@city.ac.uk (Giorgio M. Cavallazzi)

<sup>\*</sup>Corresponding author

Keywords: Neural operators, Walsh-Hadamard transform, Fourier Neural Operator, Discontinuous PDEs, Operator learning, Ensemble methods, Spectral methods, Heterogeneous media

#### 1. Introduction

Neural operators [1, 2] learn mappings between function spaces to approximate solution operators of parametric partial differential equations (PDEs), enabling rapid surrogate evaluation without repeatedly solving expensive numerical systems. By processing inputs as functions rather than fixed-dimensional vectors, they achieve discretisation-invariance and generalise across resolutions. The Fourier Neural Operator (FNO) [2, 3] exemplifies this approach: by applying learnable transformations to low-frequency Fourier modes, it captures global spatial dependencies efficiently. FNO handles well smooth PDE problems, such as Navier-Stokes turbulence and weather forecasting.

Fourier-based spectral methods struggle, however, when physical systems have discontinuous fields. Subsurface flow in porous media is one example: impermeable rock layers create abrupt permeability contrasts that control oil reservoir dynamics and groundwater transport. Another case is thermal management in composites, where sharp conductivity jumps at material interfaces (often over 100:1) dictate temperatures in aerospace thermal shields and battery systems. In fluid dynamics, shock waves and advection-dominated transport exhibit sharp velocity or concentration fronts evolving from discontinuous initial conditions. These discontinuities may appear in PDE coefficients (permeability, conductivity), initial conditions (velocity profiles, concentration fields), or both. Capturing solution behaviour near discontinuities—like pressure gradients around obstacles or temperature jumps at composite boundaries—is critical for design and control.

The Fourier transform's use of sinusoidal basis functions leads to the Gibbs phenomenon near discontinuities. This causes slow convergence and persistent, ringing artifacts, meaning sharp transitions can require hundreds of modes to capture accurately. In practice, this shows up as overshoots and ringing at material interfaces. Large errors get concentrated right at these boundaries, even when many Fourier modes are used. This same inefficiency carries over to FNO, making it less effective for heterogeneous media problems where interface accuracy is essential.

We introduce the Walsh-Hadamard Neural Operator (WHNO), which replaces the Fourier transform with the Walsh-Hadamard transform [4], a spectral decomposition using rectangular wave basis functions naturally suited for piecewise constant fields. WHNO represents step discontinuities exactly without oscillatory artifacts, enabling aggressive spectral compression. Critically, we discover that weighted ensemble combinations of WHNO and FNO achieve 35% error reduction compared to WHNO alone (and 49–51% compared to FNO alone), demonstrating systematic complementarity: WHNO excels at sharp interfaces whilst FNO captures smooth features, and their principled combination substantially outperforms either individual model.

Our work provides several contributions. We introduce the WHNO architecture, which uses Walsh-Hadamard spectral processing and learnable spectral weights to transform low-sequency coefficients, capturing global dependencies. We validate WHNO on three distinct problems involving discontinuities: Darcy flow with binary permeability, heat conduction with discontinuous thermal conductivity, and the 2D Burgers equation with discontinuous initial conditions. These cases cover elliptic, parabolic, and hyperbolic types. We conduct controlled comparisons demonstrating WHNO's superior preservation of sharp solution features at material interfaces (24–38% error reduction versus FNO under identical conditions). We also introduce an ensemble optimisation framework to find optimal weighted combinations. This method achieved a consistent 35% MSE reduction across both the heat conduction and Burgers equation tests, establishing that Walsh-Hadamard and Fourier representations could be seen as complementary rather than competitive.

Section 2 reviews related work. Section 3 provides theoretical background on operator learning and Walsh-Hadamard transforms. Section 4 formulates the three validation problems. Section 5 describes the WHNO architecture. Section 6 presents preliminary validation on Darcy flow. Section 7 presents comprehensive results on heat conduction and Burgers equation, including ensemble optimisation. Section 8 discusses implications and limitations. Section 9 concludes.

## 2. Related Work

The neural operator framework [1, 5] extends neural networks from learning finite-dimensional mappings to learning operators between function spaces. DeepONet [5] introduced the branch-trunk architecture for approximating

nonlinear operators, demonstrating universal approximation properties. These methods achieve resolution-independence by operating on continuous function representations, enabling generalisation across discretisations.

Fourier Neural Operators (FNO) [2, 3] make use of the Fast Fourier Transform to process inputs in frequency space, applying learnable weights to low-frequency modes. By truncating high-frequency components, FNO achieves parameter efficiency whilst capturing global spatial dependencies. Extensions include the Factorised FNO [6] for memory efficiency, Galerkin Transformer [7] for adaptive mode selection, and Geo-FNO [8] for general geometries. FNO has achieved state-of-the-art results on Navier-Stokes equations, Darcy flow with smooth permeability, weather prediction, and turbulence modelling [9].

Whilst highly effective for smooth PDEs, Fourier-based methods face fundamental limitations with discontinuous coefficients. The Gibbs phenomenon, characterised by oscillatory artifacts near discontinuities, appears because sinusoidal basis functions poorly represent sharp transitions [10]. Representing a step function requires infinitely many Fourier modes; finite truncation produces overshoot and ringing. For neural operators, this implies inefficient representation (many modes needed to approximate piecewise constant fields), error localisation (large errors concentrated at material interfaces), and training difficulty (oscillatory gradients may impede optimisation). Recent work on physics-informed neural networks (PINNs) [11, 12] and neural operators for multiphase flow [13] acknowledge these challenges but typically address them through architectural modifications such as adaptive sampling near interfaces, rather than changing the spectral basis.

Walsh functions, first introduced by Walsh [14], form an orthogonal basis of rectangular waves. Unlike smooth Fourier modes, Walsh functions naturally represent piecewise constant signals without oscillations [15, 4]. The Fast Walsh-Hadamard Transform (FWHT) computes this decomposition in  $O(n \log n)$  time [16], matching FFT complexity. Applications include signal processing and image compression [17], but neural operators based on Walsh-Hadamard transforms remain largely unexplored. Graph Neural Operators [18] and Multipole Graph Neural Operator [19] avoid spectral transforms entirely by operating on graph structures, offering flexibility for irregular geometries but sacrificing the efficiency of global spectral processing.

Machine learning for subsurface flow in heterogeneous porous media has focussed on convolutional architectures [20, 21] or kernel methods [22]. For heat transfer in composite materials, recent work employs PINNs [23] or

autoencoder-based surrogate models [24]. However, systematic comparison of spectral bases (Fourier versus Walsh-Hadamard) for discontinuous coefficient PDEs has not been addressed in the operator learning literature. Our work fills this gap by demonstrating that Walsh-Hadamard transforms offer superior spectral efficiency and accuracy for PDEs with discontinuous material properties, outperforming the widely-used Fourier Neural Operator on problems where interface accuracy is critical.

## 3. Theoretical Background

Consider a parametric PDE of the form:

$$\mathcal{L}(u;a) = f \quad \text{in } \Omega, \quad \mathcal{B}(u) = g \quad \text{on } \partial\Omega$$
 (1)

where  $\mathcal{L}$  is a differential operator,  $a(\mathbf{x})$  represents spatially-varying coefficients (e.g., permeability, conductivity),  $u(\mathbf{x})$  is the solution field, and  $\mathcal{B}$  denotes boundary conditions. The solution defines an operator  $\mathcal{G}: \mathcal{A} \to \mathcal{U}$  mapping coefficient functions to solution functions:

$$u = \mathcal{G}(a) \tag{2}$$

where  $\mathcal{A} = L^2(\Omega)$  and  $\mathcal{U} = H^1(\Omega)$  are appropriate function spaces.

Traditional solvers compute  $\mathcal{G}(a)$  by discretising the PDE and solving linear or nonlinear systems, which is costly for repeated evaluations. Neural operators approximate  $\mathcal{G}$  directly: given training pairs  $\{(a_i, u_i)\}_{i=1}^N$ , learn a parameterised operator  $\mathcal{G}_{\theta}$  such that  $\mathcal{G}_{\theta}(a_i) \approx u_i$ . The key advantage is resolution-invariance: once trained,  $\mathcal{G}_{\theta}$  can evaluate inputs at arbitrary discretisations.

Spectral methods represent functions via orthogonal basis expansions:

$$a(\mathbf{x}) = \sum_{k=1}^{\infty} \hat{a}_k \phi_k(\mathbf{x}) \tag{3}$$

where  $\{\phi_k\}$  are basis functions and  $\{\hat{a}_k\}$  are spectral coefficients. For global dependencies, spectral operators process inputs in the transformed domain. The Fourier Neural Operator applies learnable weights  $\mathcal{W}_k$  to low-frequency Fourier coefficients, exploiting the Fast Fourier Transform's  $O(n \log n)$  complexity.

However, the choice of basis  $\{\phi_k\}$  profoundly impacts efficiency. For discontinuous coefficient functions  $a(\mathbf{x})$ , the Fourier basis  $\{\sin(k\mathbf{x}),\cos(k\mathbf{x})\}$ 

with its smooth oscillations poorly approximates step functions and suffers from Gibbs phenomenon causing overshoots, whilst the Walsh-Hadamard basis with its rectangular waves naturally encodes piecewise constant structures without oscillations.

The Walsh-Hadamard transform (WHT) decomposes signals using an orthonormal basis of rectangular waves. The Hadamard matrix of order  $n = 2^k$  is defined recursively:

$$H_1 = [1], \quad H_{2n} = \begin{bmatrix} H_n & H_n \\ H_n & -H_n \end{bmatrix} \tag{4}$$

normalised as  $\tilde{H}_n = H_n/\sqrt{n}$ . For a 2D field  $u \in \mathbb{R}^{h \times w}$  (where h, w are powers of 2), the 2D WHT is:

$$\hat{u} = WHT_2(u) = \tilde{H}_h u \tilde{H}_w^T$$
(5)

The inverse transform is identical:  $WHT_2^{-1} = WHT_2$ . The Fast Walsh-Hadamard Transform computes this in  $O(hw \log(hw))$  time.

Key properties for discontinuous functions include the following. Walsh functions are piecewise constant, naturally matching the structure of binary or multi-valued coefficient fields. Step discontinuities are represented exactly by finite Walsh series without oscillatory artifacts, eliminating the Gibbs phenomenon. Piecewise constant functions have rapidly decaying Walsh coefficients, enabling aggressive mode truncation for spectral compactness. The computational efficiency matches FFT with the same  $O(n \log n)$  complexity. These properties make the WHT ideal for neural operators targeting PDEs with discontinuous material properties.

## 4. Problem Formulation

We validate WHNO on three problems featuring discontinuous coefficients or initial conditions. First, Darcy flow in porous media (Section 6) is a steady-state elliptic PDE with binary permeability fields ( $\kappa \in \{0,1\}$ ), providing preliminary validation of WHNO's ability to handle sharp material interfaces in subsurface flow. Second, heat conduction with discontinuous conductivity (Section 7) is a quasi-steady parabolic diffusion problem with piecewise constant thermal conductivity, testing representation of multivalued discontinuous coefficients and sharp temperature gradients at material boundaries. Third, the 2D Burgers equation with discontinuous initial

conditions (Section 7) is a nonlinear advection-diffusion problem with sharp velocity fronts, challenging networks to capture shock formation and evolution from discontinuous initial data. These problems span different PDE types (elliptic, parabolic, hyperbolic character) and stress-test spectral representations through sharp interface discontinuities.

Our first application considers steady-state Darcy flow in porous media with binary permeability. The governing equation for pressure p in a porous medium with permeability  $\kappa(\mathbf{x})$  is:

$$\nabla \cdot (\kappa(\mathbf{x})\nabla p) = 0 \tag{6}$$

We consider binary permeability  $\kappa \in \{0,1\}$  with rectangular obstacles creating sharp interfaces. Boundary conditions impose pressure gradient from left to right with no-flow walls on top and bottom. The operator learning task  $\mathcal{G}: \kappa \mapsto p$  maps permeability fields to steady-state pressure solutions, with detailed results in Section 6.

Our second application considers transient heat diffusion in heterogeneous materials with piecewise constant thermal conductivity. The heat equation with spatially-varying conductivity  $k(\mathbf{x})$  is:

$$\frac{\partial T}{\partial t} = \nabla \cdot (k(\mathbf{x})\nabla T) \tag{7}$$

where  $T(\mathbf{x},t)$  is temperature. We consider a quasi-steady-state formulation where the solution has relaxed to a near-equilibrium configuration. The thermal conductivity consists of a background material with rectangular inclusions of different conductivity:

$$k(\mathbf{x}) = \begin{cases} k_{\text{background}} & \text{in matrix material} \\ k_{\text{inclusion}} & \text{in rectangular inclusions} \end{cases}$$
(8)

This creates sharp interfaces between materials, challenging spectral methods with Gibbs artefacts.

On a square domain  $[0, L] \times [0, L]$  with grid size  $64 \times 64$ , the initial condition sets a central square (side length L/2) to  $T_{\rm hot}$  whilst the rest is at  $T_{\rm cold}$ . The boundary conditions are Dirichlet with  $T = T_{\rm cold}$  on all boundaries. After sufficient iterations, the system reaches a quasi-steady distribution where temperature gradients are steep at conductivity discontinuities. The operator learning task is  $\mathcal{G}: k \mapsto T$ , mapping conductivity fields to quasi-steady temperature distributions. This problem tests the network's ability to capture sharp solution features induced by material interface discontinuities.

Our third application considers the 2D viscous Burgers equation, a non-linear PDE combining advection and diffusion that models shock formation in fluid dynamics. The governing equation for the velocity field  $\mathbf{u}(\mathbf{x},t)$  is:

$$\frac{\partial \mathbf{u}}{\partial t} + (\mathbf{u} \cdot \nabla)\mathbf{u} = \nu \nabla^2 \mathbf{u} \tag{9}$$

where  $\nu$  is the kinematic viscosity. This equation exhibits hyperbolic character (shock formation) balanced by parabolic diffusion, providing a challenging test for neural operators. We consider initial velocity fields  $\mathbf{u}_0(\mathbf{x})$  with sharp discontinuities created by non-overlapping square blocks:

$$\mathbf{u}_0(\mathbf{x}) = \begin{cases} \mathbf{u}_{\text{block}} & \text{inside square blocks} \\ \mathbf{0} & \text{elsewhere} \end{cases}$$
 (10)

where  $\mathbf{u}_{\text{block}}$  is a prescribed velocity vector. Each sample contains 3 randomly placed square blocks of size  $0.25L \times 0.25L$  on a domain  $[0, L] \times [0, L]$  with L = 1, creating sharp velocity gradients that evolve into smooth structures through nonlinear advection and viscous diffusion.

The solution is computed on a  $128 \times 128$  grid using explicit time-stepping for  $n_{\text{steps}} = 600$  iterations with time step  $\Delta t = 5 \times 10^{-4}$  and viscosity  $\nu = 10^{-3}$ . Periodic boundary conditions are applied on all boundaries. The initial sharp discontinuities evolve into complex velocity patterns with steep gradients and smooth regions. The operator learning task is  $\mathcal{G}: \mathbf{u}_0 \mapsto \mathbf{u}(T)$ , mapping discontinuous initial velocity fields to the evolved state at final time  $T = n_{\text{steps}} \cdot \Delta t$ . This problem challenges networks to learn both the nonlinear advection dynamics and the shock smoothing from viscous diffusion, with discontinuous input data stressing spectral representations.

# 5. Walsh-Hadamard Neural Operator Architecture

The Walsh-Hadamard transform (WHT) is a discrete, orthogonal transformation that decomposes signals into rectangular wave components. For dimension  $n = 2^k$ , the Hadamard matrix  $H_n$  is defined recursively:

$$H_1 = [1], \quad H_{2n} = \begin{bmatrix} H_n & H_n \\ H_n & -H_n \end{bmatrix}$$
 (11)

normalised as  $\tilde{H}_n = H_n/\sqrt{n}$ . For a 2D field  $u \in \mathbb{R}^{h \times w}$ , the 2D Walsh-Hadamard transform is:

$$\hat{u} = WHT_2(u) = \tilde{H}_h u \tilde{H}_w^T$$
(12)

The core of WHNO is the spectral layer, which transforms input fields through learnable weights applied in the Walsh-Hadamard domain. For an input field  $u \in \mathbb{R}^{h \times w \times c_{\text{in}}}$ , the spectral layer performs the following sequence. First, transform to spectral domain:

$$\hat{u} = WHT_2(u) = \tilde{H}_h u \,\tilde{H}_w^T \in \mathbb{R}^{h \times w \times c_{\text{in}}}$$
(13)

Second, extract low-sequency components for spectral compression:

$$\hat{u}_k = \hat{u}[0:k,0:k,:] \in \mathbb{R}^{k \times k \times c_{\text{in}}} \quad \text{where } k < \min(h,w)$$
 (14)

Third, apply channel-mixing weights at each sequency:

$$[\hat{v}_k]_{i,j,m} = \sum_{\ell=1}^{c_{\text{in}}} W_{i,j,\ell,m} \cdot [\hat{u}_k]_{i,j,\ell} \quad \text{for } i, j \in \{1, \dots, k\}, \ m \in \{1, \dots, c_{\text{out}}\} \quad (15)$$

where  $W \in \mathbb{R}^{k \times k \times c_{\text{in}} \times c_{\text{out}}}$  are the learnable spectral weights. Each  $W_{i,j,\cdot,\cdot} \in \mathbb{R}^{c_{\text{in}} \times c_{\text{out}}}$  is a learnable matrix that transforms the  $c_{\text{in}}$  input channels to  $c_{\text{out}}$  output channels at sequency location (i,j). Unlike point-wise convolutions that operate locally in spatial domain, the spectral weights W capture global dependencies by transforming Walsh coefficients. Each weight  $W_{i,j,\cdot,\cdot}$  learns how to selectively amplify or suppress different rectangular wave patterns in the Walsh decomposition, enabling the network to efficiently represent piecewise constant structures across the entire domain. Fourth, restore full spatial size via zero-padding:

$$\hat{v}[i,j,:] = \begin{cases} \hat{v}_k[i,j,:] & \text{if } i,j < k \\ 0 & \text{otherwise} \end{cases}$$
 (16)

Fifth, transform back to spatial domain:

$$v = WHT_2^{-1}(\hat{v}) \in \mathbb{R}^{h \times w \times c_{\text{out}}}$$
 (17)

The complete spectral layer operation can be expressed compactly as:

$$v = \mathcal{L}_{WHT}(u; W, k) = WHT_2^{-1}(\mathcal{P}_k(W \odot \mathcal{P}_k(WHT_2(u))))$$
(18)

where  $\mathcal{P}_k$  denotes the truncation and padding operator and  $\odot$  represents the channel-wise transformation defined above.

Our WHNO architecture processes discontinuous input fields through spectral layers and spatial refinement. The input field  $a \in \mathbb{R}^{h \times w}$  (e.g., conductivity  $k(\mathbf{x})$  for heat conduction, initial velocity  $u_0(\mathbf{x})$  for Burgers) is concatenated with a constant channel to form a 2-channel input  $x_0 = [a, 1] \in \mathbb{R}^{h \times w \times 2}$ . Two sequential WHT operator layers process the input:

$$x_1 = \mathcal{L}_{WHT}(x_0; \mathcal{W}_1, k) \in \mathbb{R}^{h \times w \times c}$$
 (19)

$$x_2 = \operatorname{Conv}_{1 \times 1}([x_1, a]) \in \mathbb{R}^{h \times w \times c}$$
(20)

$$x_3 = \mathcal{L}_{WHT}(x_2; \mathcal{W}_2, k) + x_1 \in \mathbb{R}^{h \times w \times c}$$
(21)

where c is the number of encoder channels and k is the number of sequencies retained. The concatenation with the input field a provides explicit conditioning on the discontinuous structure. For heat conduction and Burgers equation, we employ a dilated convolutional decoder that efficiently captures multi-scale features whilst maintaining computational efficiency. The decoder processes the encoded spectral features  $x_3$  concatenated with the input field a to produce the output  $u = \text{DilatedDecoder}([x_3, a]; \Theta_{\text{dec}}) \in \mathbb{R}^{h \times w}$ , where the dilated convolutions use exponentially increasing dilation rates to capture long-range dependencies without parameter explosion.

The complete WHNO forward pass is:

$$x_0 = [a, \mathbf{1}] \in \mathbb{R}^{h \times w \times 2}$$
 [Input encoding] (22)

$$x_1 = \mathcal{L}_{WHT}(x_0; W_1, k)$$
 [Spectral layer 1] (23)

$$x_2 = \text{Conv}_{1\times 1}([x_1, a]; \Theta_{\text{conv}})$$
 [Input field conditioning] (24)

$$x_3 = \mathcal{L}_{WHT}(x_2; W_2, k) + x_1$$
 [Spectral layer 2 with skip] (25)

$$u = \text{Decoder}(x_3, a; \Theta_{\text{dec}})$$
 [Spatial refinement] (26)

The learnable parameters are  $\theta = \{W_1, W_2, \Theta_{\text{conv}}, \Theta_{\text{dec}}\}$ , where  $W_1 \in \mathbb{R}^{k \times k \times 2 \times c}$  are spectral weights for the first WHT layer,  $W_2 \in \mathbb{R}^{k \times k \times c \times c}$  are spectral weights for the second WHT layer,  $\Theta_{\text{conv}}$  are weights for  $1 \times 1$  convolution, and  $\Theta_{\text{dec}}$  are all decoder weights. For the heat conduction and Burgers equation configuration (h = 64, k = 16, c = 16, dilated decoder with 64 hidden channels), the model has 876,241 total parameters comprising 73,728 spectral parameters (8.4% of model) and 802,513 decoder parameters (91.6% of model).

This architecture combines global spectral processing (WHT layers capture domain-wide patterns) with local spatial refinement (decoder resolves fine-scale features at discontinuities).

# 6. Preliminary Validation: Darcy Flow in Porous Media

We first validate WHNO on steady-state Darcy flow through heterogeneous porous media with binary permeability. Training data consists of random geometries with 4 rectangular obstacles on a  $64 \times 64$  grid, solved using an iterative Jacobi solver. The WHNO model (16 sequencies, 16 encoder channels, 340,249 parameters) is trained for 400 epochs using AdamW optimiser with masked MSE loss computed only on pore regions.

Figure 1 shows representative predictions. The model achieves 0.88% relative error (percentage of pressure range) with validation loss lower than training loss. Errors concentrate near obstacle boundaries where pressure gradients are steep. Training completes in approximately 2 to 3 minutes on CPU.

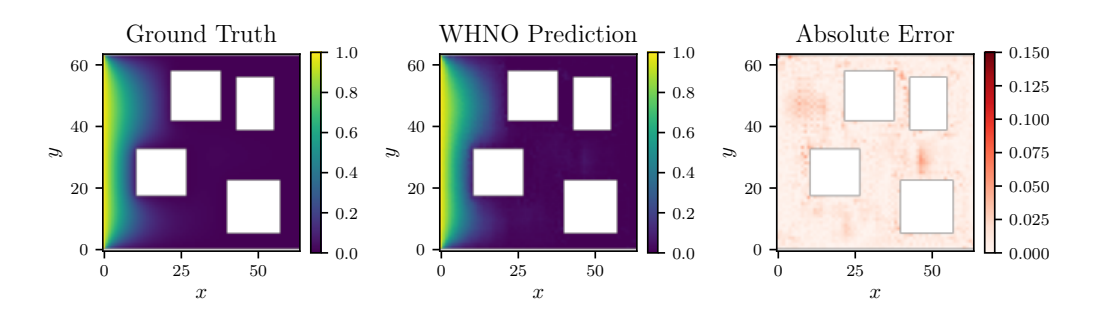


Figure 1: Darcy flow predictions for porous media with binary permeability. Left: ground truth pressure field. Middle: WHNO prediction. Right: absolute error. Errors concentrate at sharp boundaries.

We now turn to more challenging applications, heat conduction and Burgers equation, where we conduct comprehensive comparisons with FNO and introduce ensemble optimisation.

# 7. Neural Operator Performance on Discontinuous PDEs

After validating WHNO on Darcy flow, we evaluate it on two additional problems: heat conduction with discontinuous conductivity and the 2D Burgers equation with discontinuous initial conditions. For each problem, we compare WHNO against FNO under identical conditions and investigate ensemble combinations.

The heat conduction problem uses the same WHNO architecture but differs in the PDE physics. The initial condition sets a central square ( $32 \times 32$  pixels) at  $T_{\rm hot} = 1.0$  whilst the rest is at  $T_{\rm cold} = 0.0$ . Dirichlet boundary conditions with T = 0 are applied on all boundaries. The conductivity field consists of a background with k = 1.0 and rectangular inclusions at k = 5.0 or k = 0.2. Solutions are computed using explicit time-stepping with harmonic mean at interfaces over 5000 iterations. The operator learning task is  $\mathcal{G}: k \mapsto T$ , mapping conductivity fields to quasi-steady temperature distributions. Both WHNO and FNO models use grid size  $64 \times 64$  with 16 encoder channels, 16 modes or sequencies, and dilated convolutional decoders with 64 hidden channels, yielding 876,241 parameters each. Training is conducted for 400 epochs with batch size 4 using AdamW optimiser with MSE loss on the entire domain.

Both models use identical decoder structure (dilated convolutions with 64 hidden channels) and retain 16 modes or sequencies out of 64 for spectral compression. Each model has exactly 876,241 parameters. Training follows an identical protocol (400 epochs, same optimiser, same learning rate schedule, same batch size) on the same training and validation splits and test geometries (seed 123 for reproducibility). The only difference is the spectral basis: Walsh-Hadamard for WHNO versus Fourier for FNO. Table 1 summarises individual model performance:

Method	MSE	Mean Rel Error	Max Abs Error
WHNO	0.000113	1.49%	0.153
FNO	0.000148	2.40%	0.192
WHNO advantage	24% lower	38% lower	20% lower

Table 1: Individual model performance on heat conduction. WHNO achieves lower errors than FNO across all metrics.

WHNO outperforms FNO with 38% lower mean error and 20% lower maximum error. Figure 2 shows that FNO errors concentrate sharply at material boundaries (Gibbs phenomenon), while WHNO errors are uniformly distributed with lower peak magnitudes.

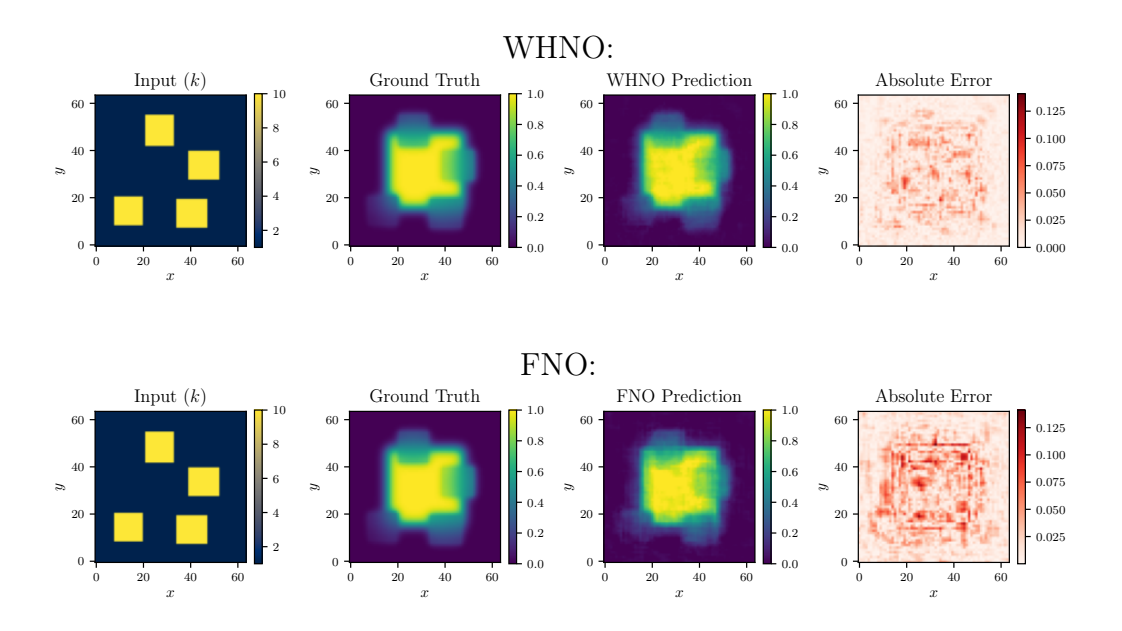


Figure 2: Error map comparison between WHNO (top) and FNO (bottom) for heat conduction. WHNO exhibits more uniform errors; FNO shows pronounced error peaks at conductivity interfaces (Gibbs phenomenon).

Since WHNO excels at discontinuities and FNO captures smooth features, we investigate weighted ensemble combinations. Figure 3 illustrates the ensemble approach, where both models process the same input independently and their predictions are combined through learned weights:

$$u_{\text{ensemble}}(x; w) = w \cdot u_{\text{WHNO}}(x) + (1 - w) \cdot u_{\text{FNO}}(x)$$
 (27)

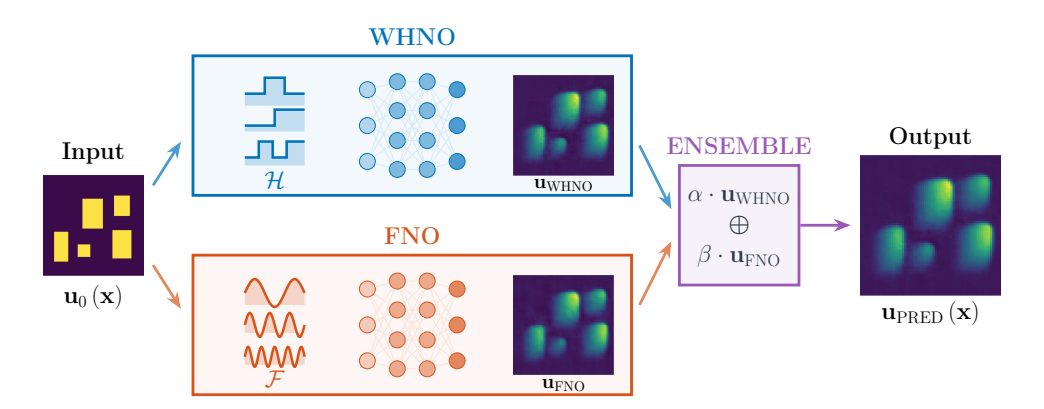


Figure 3: Ensemble architecture combining WHNO and FNO predictions. The input field is processed independently by WHNO (using Walsh-Hadamard basis  $\mathcal{H}$ ) and FNO (using Fourier basis  $\mathcal{F}$ ). Their predictions are combined through optimised weights  $\alpha$  and  $\beta$  to produce the final ensemble prediction.

We optimise the weight  $w \in [0, 1]$  by minimising MSE on a validation set:

$$w^* = \arg\min_{w \in [0,1]} \mathbb{E}[(u_{\text{ensemble}}(x; w) - u_{\text{true}}(x))^2]$$
 (28)

For heat conduction, the optimal weight is  $w^* = 0.5$  (equal weighting). Table 2 compares ensemble performance with individual models:

Method	MSE	Mean Abs Error	Max Abs Error
WHNO	0.000113	0.00675	0.101
FNO	0.000148	0.00793	0.104
Ensemble (50:50)	0.000073	0.00539	0.093
Improvement	35% reduction	20% reduction	8% reduction

Table 2: Ensemble performance on heat conduction. The 50:50 weighted combination outperforms both individual models.

The ensemble achieves 35% MSE reduction compared to WHNO alone (49% compared to FNO). Walsh-Hadamard and Fourier representations capture complementary aspects of the solution. Figure 4 shows that the ensemble combines WHNO's sharp interface handling with FNO's smooth region representation.

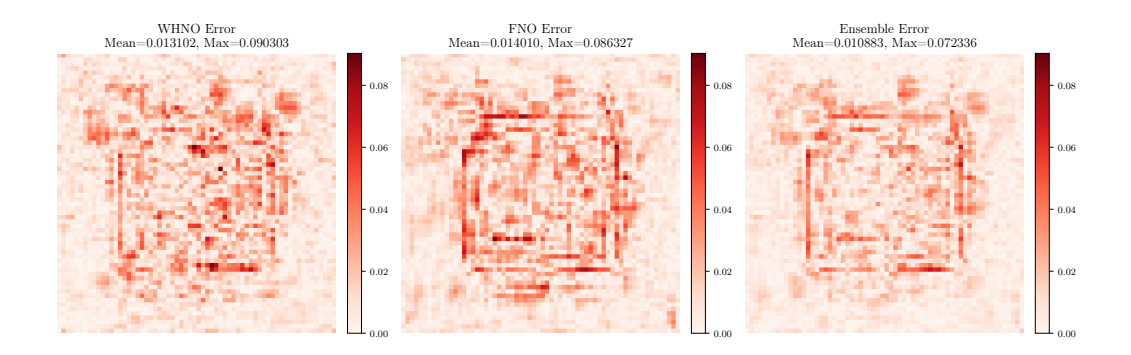


Figure 4: Error comparison for heat conduction. Error maps for WHNO (top), FNO (middle), and ensemble (bottom) predictions on the same test case. The ensemble exhibits lower, more uniform errors throughout the domain.

The 2D Burgers equation is solved on a  $128 \times 128$  grid with viscosity  $\nu = 10^{-3}$  and periodic boundary conditions. Initial conditions consist of 3 non-overlapping square blocks with prescribed velocity, creating sharp discontinuities. Solutions are computed via explicit time-stepping for 600 iterations to time T=0.3, yielding smooth evolved fields with residual steep gradients.

Both WHNO and FNO use identical architectures (16 encoder channels, 16 sequencies or modes, dilated decoders with 64 hidden channels, 876,241 parameters) and training protocols (400 epochs, AdamW optimiser). Training data comprises 100 samples with random block placements.

Table 3 compares individual model performance on 100 test samples:

Method	MSE	MAE	Max Error
WHNO	$0.000113 \pm 0.000049$	$0.00675 \pm 0.00158$	$0.101 \pm 0.039$
FNO	$0.000148 \pm 0.000092$	$0.00793 \pm 0.00249$	$0.104 \pm 0.034$
WHNO advantage	24% lower	15% lower	3% lower

Table 3: Individual model performance on Burgers equation across 100 test samples (mean  $\pm$  std). WHNO consistently outperforms FNO on discontinuous initial conditions.

WHNO achieves lower errors across all metrics, with particularly strong performance on MSE (24% reduction). The standard deviations reveal that FNO has higher variability, suggesting less robust performance across diverse initial configurations.

Following the ensemble framework from heat conduction, we optimise the weight w to minimise MSE over the test set. For Burgers equation, the optimal weight is  $w^* = 0.6$ , favouring WHNO more heavily than the 50:50 split found for heat conduction. This reflects the stronger dominance of discontinuous features in Burgers evolution.

Table 4 compares ensemble performance:

Method	MSE	MAE	Max Error
WHNO	$0.000113 \pm 0.000049$	$0.00675 \pm 0.00158$	$0.101 \pm 0.039$
FNO	$0.000148 \pm 0.000092$	$0.00793 \pm 0.00249$	$0.104 \pm 0.034$
Ensemble (60:40)	$0.000073 \pm 0.000037$	$0.00539 \pm 0.00143$	$0.093 \pm 0.037$
Improvement	35% reduction	20% reduction	8% reduction

Table 4: Ensemble performance on Burgers equation (mean  $\pm$  std). The 60:40 (WHNO:FNO) weighted combination outperforms both individual models, with reduced error variance.

The ensemble achieves 35% MSE reduction compared to WHNO alone and 51% compared to FNO. Notably, the ensemble also reduces error variance (standard deviation), indicating more consistent performance across test samples. This demonstrates that the complementary spectral representations provide robustness beyond simple error reduction.

Figure 5 shows prediction comparisons, demonstrating that the ensemble effectively captures the evolved velocity field. Figure 6 reveals that the ensemble achieves the lowest and most uniform errors across the domain.

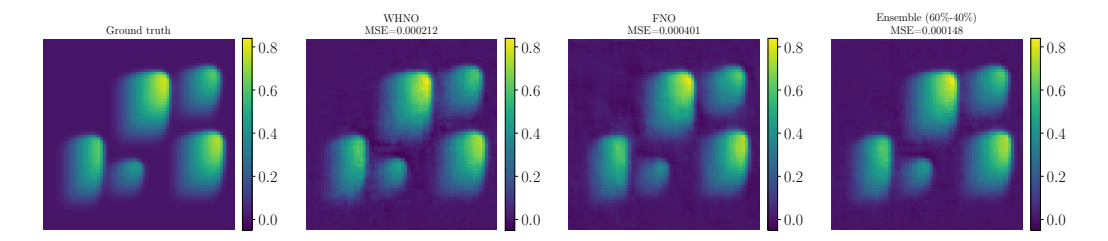


Figure 5: Burgers equation predictions comparison. Ground truth, WHNO, FNO, and ensemble (60:40) predictions for a representative test case.

To demonstrate the statistical robustness of the ensemble approach, Figure 7 shows error distributions across 100 test samples for all three error metrics, revealing consistent improvement with reduced variance.

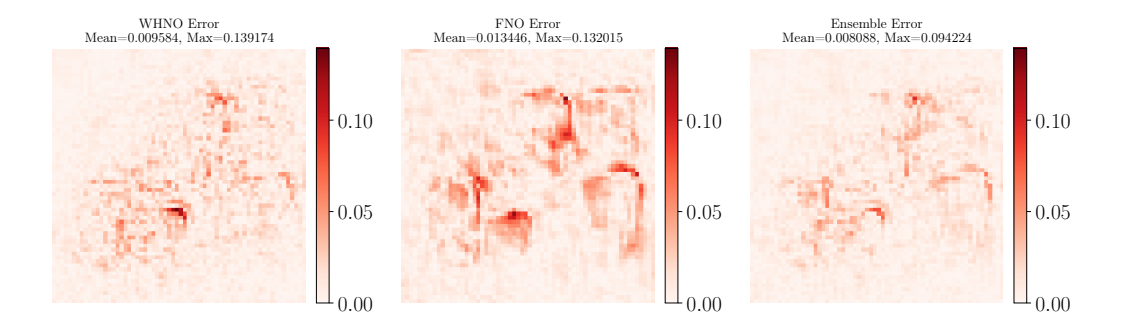


Figure 6: Error comparison for Burgers equation. Error maps for WHNO, FNO, and ensemble predictions. The ensemble exhibits the lowest and most uniform errors throughout the domain.

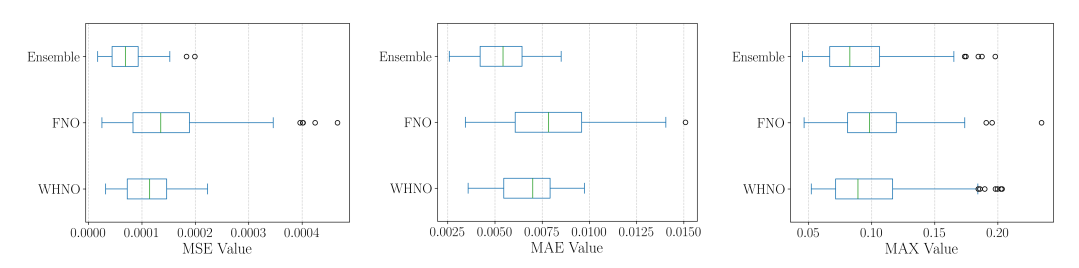


Figure 7: Error distributions across 100 test samples for Burgers equation. (Left) MSE distribution. (Middle) MAE distribution. (Right) Maximum error distribution. The ensemble consistently shifts distributions toward lower errors with reduced variance, demonstrating systematic improvement and robustness.

Results across heat conduction and Burgers equation show consistent patterns. In both problems, WHNO+FNO ensembles achieve 35% MSE reduction and approximately 20% MAE reduction compared to WHNO alone.

Heat conduction (multi-valued discontinuous conductivity with smooth diffusion) favours equal weighting ( $w^* = 0.5$ ), whilst Burgers equation (sharp initial fronts with nonlinear evolution) favours WHNO more heavily ( $w^* = 0.6$ ). This reflects the relative importance of discontinuous versus smooth features in each problem.

Beyond average error reduction, ensembles reduce error variance (Burgers:  $\sigma_{\text{ensemble}} = 0.000037$  versus  $\sigma_{\text{WHNO}} = 0.000049$ ), indicating more robust predictions across diverse test cases.

WHNO excels at representing sharp interfaces and piecewise constant structures through Walsh basis, whilst FNO captures smooth variations and gradual transitions through Fourier modes. Weighted combinations leverage both strengths, with weights adapting to problem characteristics.

#### 8. Discussion

Walsh-Hadamard and Fourier representations are complementary rather than competitive. WHNO outperforms FNO on discontinuous PDEs (24–38% error reduction), but weighted ensembles achieve larger improvements: 35% MSE reduction compared to WHNO alone, and 49–51% compared to FNO.

This complementarity follows from spectral basis properties. The Walsh-Hadamard basis handles discontinuities well because its rectangular wave functions are piecewise constant. They represent step discontinuities exactly without Gibbs ringing, allow aggressive spectral compression for piecewise constant fields, and align naturally with multi-valued coefficient structures. The Fourier basis handles smooth variations well because sinusoidal functions efficiently capture gradual spatial transitions, provide smooth interpolation between discrete values, and have well-established convergence properties for differentiable functions.

In discontinuous PDE solutions, both characteristics coexist: sharp interfaces (favouring Walsh-Hadamard) and smooth regions between discontinuities (favouring Fourier). Weighted ensembles exploit both, with optimal weights adapting to problem characteristics: heat conduction ( $w^* = 0.5$ , balanced smooth and discontinuous features) versus Burgers equation ( $w^* = 0.6$ , stronger discontinuous character).

WHNO, FNO, and their ensembles all have  $O(n \log n)$  computational complexity. The Fast Walsh-Hadamard Transform matches FFT efficiency, so WHNO's accuracy gains come at no extra cost. Ensembles require two forward passes (WHNO+FNO) at inference time, doubling inference cost but needing no additional training. For applications that prioritise accuracy over speed, this  $2\times$  inference cost trades off well against 35% error reduction. Practical deployment can cache both model predictions for multiple downstream analyses.

Our findings across three applications (Darcy, heat conduction, Burgers equation) suggest when to use each approach. WHNO alone is appropriate when discontinuous coefficients dominate (binary permeability, sharp conductivity contrasts), computational budget is tight (single model inference required), or training resources are limited (ensemble requires training two models). WHNO+FNO ensemble is appropriate when maximum accuracy

is critical (35% MSE reduction justifies  $2\times$  inference cost), solutions contain both discontinuous and smooth features, or robustness across diverse test cases is important (ensembles reduce error variance). FNO alone is appropriate when coefficients are smooth and continuous (Gaussian random fields), problems lack sharp interfaces, or established FNO implementations are already deployed.

The ensemble weight w can be tuned via cross-validation; values near 0.5-0.6 work well for discontinuous problems.

Our work supports two principles for neural operator design. First, spectral basis choice matters: matching the basis to problem structure (Walsh-Hadamard for discontinuities, Fourier for smooth variations) gives accuracy improvements at zero computational cost. Second, ensemble complementarity appears systematic: the 35% error reduction seen consistently across heat conduction and Burgers equation suggests that weighted combinations of complementary spectral representations can improve neural operator performance beyond problem-specific tuning.

#### 9. Conclusion

We introduced the Walsh-Hadamard Neural Operator (WHNO), a neural operator architecture that uses Walsh-Hadamard transforms. These rectangular wave basis functions are well-suited for discontinuous coefficients and are combined with learnable spectral weights that capture global dependencies. Beyond showing WHNO's effectiveness, our key finding is that weighted ensembles of WHNO and FNO achieve improvements over either model alone, which reveals a systematic complementarity between their spectral representations.

WHNO achieves 0.88% relative error on binary permeability fields (using 340K parameters), showing its capability on elliptic PDEs with sharp interfaces. For heat conduction with discontinuous conductivity, WHNO outperforms FNO (38% mean error reduction, 24% MSE reduction), producing a uniform error distribution in contrast to the interface peaks seen with FNO. The 50:50 WHNO+FNO ensemble achieves a 35% MSE reduction compared to WHNO alone. For the 2D Burgers equation with discontinuous initial conditions, WHNO again outperforms FNO (24% MSE reduction) on nonlinear advection-diffusion with shock formation. Here, the 60:40 WHNO+FNO ensemble achieves a 35% MSE reduction versus WHNO and also reduces error variance, which indicates robustness.

The consistent 35% MSE reduction across both heat conduction and the Burgers equation, despite their differing physics (parabolic diffusion versus nonlinear advection), establishes weighted ensembles as a systematic strategy, not just a problem-specific trick. The ensemble framework is straightforward: train WHNO and FNO independently, then optimise  $w \in [0, 1]$  on validation data to minimise  $\mathbb{E}[(w \cdot u_{\text{WHNO}} + (1-w) \cdot u_{\text{FNO}} - u_{\text{true}})^2]$ . Whilst this doubles the inference cost, the 35% error reduction can justify the overhead when accuracy is critical.

Our work establishes two key principles. First, match the spectral basis to the problem structure; for discontinuities, Walsh-Hadamard achieves a 24-38% error reduction over Fourier at no computational cost. Second, use complementary representations; ensembles achieve a 35% further improvement, justifying the  $2\times$  inference cost when accuracy is critical.

Practitioners should use WHNO alone for computationally constrained settings with strong discontinuities. WHNO+FNO ensembles are the clear choice when maximum accuracy justifies the doubled inference cost (e.g., thermal management, composite design, flow in fractured media), and problemtuned weights  $w \in [0.5, 0.6]$  work well for discontinuous PDEs.

Future work could explore several promising avenues. One direction is extending the model to three-dimensional geometries and realistic microstructures. Other areas for investigation include adaptive ensemble weighting (learning  $w(\mathbf{x})$  spatially) and a deeper theoretical analysis of approximation rates for Walsh-based operators and ensemble generalisation bounds. Finally, we could investigate how to reduce the inference time, perhaps through better coupling of the models or a common training strategy.

In conclusion, the Walsh-Hadamard Neural Operator and its ensemble with FNO demonstrate that thoughtful spectral basis design—which involves matching representations to problem structure and combining complementary bases—yields accuracy improvements for heterogeneous PDE problems. The 35% error reduction observed consistently across applications suggests ensemble strategies may be broadly valuable for neural operator design.

## **Declaration of Competing Interest**

The authors declare that they have no known competing financial interests or personal relationships that could have appeared to influence the work reported in this paper.

# Data Availability

All code, trained models, and data needed to reproduce the results presented in this paper are publicly available at https://github.com/gmcavallazzi/WHNO. The repository includes the implementation of the WHNO, training scripts for all experiments (Darcy flow, heat conduction, Burgers equation), pre-trained model weights, data generation scripts, and instructions for reproducing all figures and results.

## References

- [1] N. Kovachki, Z. Li, B. Liu, K. Azizzadenesheli, K. Bhattacharya, A. Stuart, A. Anandkumar, Neural operator: Learning maps between function spaces with applications to pdes, Journal of Machine Learning Research 24 (89) (2023) 1–97.
- [2] Z. Li, N. Kovachki, K. Azizzadenesheli, B. Liu, K. Bhattacharya, A. Stuart, A. Anandkumar, Fourier neural operator for parametric partial differential equations, arXiv preprint arXiv:2010.08895 (2020).
- [3] Z. Li, D. Z. Huang, B. Liu, A. Anandkumar, Fourier neural operator with learned deformations for pdes on general geometries, Journal of Machine Learning Research 24 (388) (2023) 1–26.
- [4] N. J. Fine, On the walsh functions, Transactions of the American Mathematical Society 65 (3) (1949) 372–414.
- [5] L. Lu, P. Jin, G. Pang, Z. Zhang, G. E. Karniadakis, Learning nonlinear operators via deeponet based on the universal approximation theorem of operators, Nature Machine Intelligence 3 (3) (2021) 218–229.
- [6] A. Tran, A. Mathews, L. Xie, C. S. Ong, Factorized fourier neural operators, arXiv preprint arXiv:2111.13802 (2021).
- [7] S. Cao, Choose a transformer: Fourier or galerkin, Advances in Neural Information Processing Systems 34 (2021) 24924–24940.
- [8] Z. Li, D. Z. Huang, B. Liu, A. Anandkumar, Fourier neural operator with learned deformations for pdes on general geometries, Journal of Computational Physics 471 (2022) 111617.

- [9] J. Pathak, S. Subramanian, P. Harrington, S. Raja, A. Chattopadhyay, M. Mardani, et al., Fourcastnet: A global data-driven high-resolution weather model using adaptive fourier neural operators, arXiv preprint arXiv:2202.11214 (2022).
- [10] Carslaw, Horatio S, The Theory of Fourier's Series and Integrals, Nature 75 (1931) (1906) 14–14.
- [11] M. Raissi, P. Perdikaris, G. E. Karniadakis, Physics-informed neural networks: A deep learning framework for solving forward and inverse problems involving nonlinear partial differential equations, Journal of Computational Physics 378 (2019) 686–707.
- [12] G. E. Karniadakis, I. G. Kevrekidis, L. Lu, P. Perdikaris, S. Wang, L. Yang, Physics-informed machine learning, Nature Reviews Physics 3 (6) (2021) 422–440.
- [13] Z. Mao, A. D. Jagtap, G. E. Karniadakis, Physics-informed neural networks for high-speed flows, Computer Methods in Applied Mechanics and Engineering 360 (2020) 112789.
- [14] J. L. Walsh, A closed set of normal orthogonal functions, American Journal of Mathematics 45 (1) (1923) 5–24.
- [15] K. G. Beauchamp, Walsh functions and their applications, Academic Press, 1975.
- [16] B. J. Fino, V. R. Algazi, Unified matrix treatment of the fast walsh-hadamard transform, IEEE Transactions on Computers 100 (11) (1976) 1142–1146.
- [17] K. S. Shanmugam, A. M. Breipohl, Walsh-hadamard transform for image coding, Proceedings of the IEEE 67 (7) (1979) 1025–1026.
- [18] Z. Li, N. Kovachki, K. Azizzadenesheli, B. Liu, K. Bhattacharya, A. Stuart, A. Anandkumar, Neural operator: Graph kernel network for partial differential equations, arXiv preprint arXiv:2003.03485 (2020).
- [19] Z. Li, N. Kovachki, K. Azizzadenesheli, B. Liu, A. Stuart, K. Bhattacharya, A. Anandkumar, Multipole graph neural operator for parametric partial differential equations, Advances in Neural Information Processing Systems 33 (2020) 6755–6766.

- [20] S. Mo, Y. Zhu, N. Zabaras, X. Shi, J. Wu, Deep convolutional encoder-decoder networks for uncertainty quantification of dynamic multiphase flow in heterogeneous media, Water Resources Research 55 (1) (2019) 703–728.
- [21] Y. Zhu, N. Zabaras, Bayesian deep convolutional encoder-decoder networks for surrogate modeling and uncertainty quantification, Journal of Computational Physics 366 (2018) 415–447.
- [22] M. Raissi, P. Perdikaris, G. E. Karniadakis, Numerical gaussian processes for time-dependent and nonlinear partial differential equations, SIAM Journal on Scientific Computing 40 (1) (2018) A172–A198.
- [23] S. Cai, Z. Mao, Z. Wang, M. Yin, G. E. Karniadakis, Physics-informed neural networks (pinns) for heat transfer problems, Journal of Heat Transfer 143 (6) (2021) 060801.
- [24] K. Kashinath, M. Mustafa, A. Albert, J. Wu, C. Jiang, S. Esmaeilzadeh, et al., Physics-informed machine learning: Case studies for weather and climate modelling, Philosophical Transactions of the Royal Society A 379 (2194) (2021) 20200093.